Concentration phenomena in the geometry of Bell correlations

Cristhiano Duarte,[1,2] Samuraí Brito,[1] Barbara Amaral,[1,3] and Rafael Chaves[1,4]

[1]*International Institute of Physics, Federal University of Rio Grande do Norte, 59070-405 Natal, Rio Grande do Norte, Brazil*

[2]*Schmid College of Science and Technology, Chapman University, One University Drive, Orange, California 92866, USA*

[3]*Departamento de Física e Matemática, Campus Alto Paraopeba, Universidade Federal de São João del-Rei, 36.420-000 Ouro Branco, Minas Gerais, Brazil*

[4]*School of Science and Technology, Federal University of Rio Grande do Norte, 59078-970 Natal, Rio Grande do Norte, Brazil*

(Received 8 October 2018; published 19 December 2018)

Bell's theorem shows that local measurements on entangled states give rise to correlations incompatible with local-hidden-variable models. The degree of quantum nonlocality is not maximal though, as there are even more nonlocal theories beyond quantum theory still compatible with the nonsignaling principle. In spite of decades of research, we still have a very fragmented picture of the whole geometry of these different sets of correlations. Here we employ both analytical and numerical tools to ameliorate that. First, we identify two different classes of Bell scenarios where the nonsignaling correlations can behave very differently: In one case, the correlations are generically quantum and nonlocal while in the other quite the opposite happens as the correlations are generically classical and local. Second, by randomly sampling over nonsignaling correlations, we compute the distribution of a nonlocality quantifier based on the trace distance to the local set. With that we conclude that the nonlocal correlations can show a concentration phenomenon: Their distribution is peaked at a distance from the local set that increases both with the number of parts or measurements being performed.

DOI: 10.1103/PhysRevA.98.062114

I. INTRODUCTION

Bell nonlocality [1], the fact that local measurements on some entangled states give rise to correlations incompatible with local-hidden-variable models, has become one of the cornerstones in our modern understanding of quantum theory. Beyond its fundamental role, it is also at the core of many relevant applications in information processing such as quantum cryptography [2–5], randomness certification [6,7], self-testing [8–10], dimension witnesses [11–13], and communication complexity problems [14–16].

Despite being more than five decades old, Bell's theorem still offers a number of experimental and theoretical challenges. It was only recently that the violation of a Bell inequality has been unambiguously confirmed experimentally [17–20]. From the theoretical perspective, very general frameworks have been developed [21,22] including generalizations of Bell's original simple scenario, consisting of two distant parts making two possible dichotomic measurements, to more measurements, outcomes, and parts [23–25], sequential measurement scenarios [26,27], scenarios with communication [28–34], and complex networks [35,36]. However, still very basic questions remain unsolved. At the center of many open problems is the fact that there exist correlations agreeing with relativistic causality, the so-called nonsignaling (NS) correlations, which are incompatible with quantum predictions [37,38] though. Understanding how to recover the set of quantum correlations and more generally how to obtain a more refined picture of its relation to the sets of local or classical and nonsignaling correlations remains a very active field of research [39–44].

In a typical Bell scenario with a finite number of parts, measurements, and outcomes, testing whether a given observed correlation falls into the nonsignaling set is a computationally simple task, as it basically amounts to testing finitely many linear constraints [22]. On the other hand, testing whether a correlation is local or quantum is considerably more difficult. It is known that the set of local correlations is a convex polytope [21] and as such can be characterized by finitely many extremal points or equivalently [45,46] finitely many linear inequalities (the nontrivial of which are known as Bell inequalities). While we can easily list such extremal points, obtaining the Bell inequalities is a notoriously thorny issue, the complexity of which grows very fast as the Bell scenario of interest becomes less simple. With the extremal points of the polytope we can in principle test the locality of a given correlation, but once more the complexity grows very fast and indeed this is a problem known to be intrinsically difficult, as it stands in the NP-hard complexity class [21]. Finally, testing whether a given correlation admits a quantum realization is even harder. The best known solution is given by a hierarchy of semidefinite programs that converges asymptotically to the quantum set [47,48]. The still very fragmented picture of the geometry associated with the correlations sets comes from the inherent hardness that characterizes them [49].

One way of getting around to such difficulties while gathering at least partial information about the local, quantum, and NS sets is to consider their relative volumes [50,51]. More recently, machine learning techniques have also been employed [52]. Another promising venue has been to employ probabilistic and sampling techniques [53–56]. For instance, in Ref. [53], estimating both the quantum norm and the classical norm of random matrices with biorthogonally invariant probability distributions, the authors proved that full correlators arising from local measurements on a pure bipartite quantum

system are generically nonlocal. If instead the full probability distributions are considered [56], then the probability to find an N-partite qudit system violating any Bell inequality goes to zero, asymptotically in N, provided that $d > mv(2m-1)^2$, where m is the number of measurements per party, v is the number of outcomes per measurement, and d is dimension of the associated Hilbert space.

Employing both numerical and analytical tools, in this paper we provide further insight into the geometry of the set of correlations arising in Bell scenarios. First, considering a bipartite Bell scenario with an increasing number m of dichotomic measurements and using the probabilistic approach (as discussed, for example, in [57]), we prove that nonsignaling full correlators are generically nonlocal and quantum. This means that the volume of the local set tends to zero, whereas the volume of those correlations with quantum realization fills the entire nonsignaling region. Surprisingly, we also noticed that for a particular bipartite Bell scenario connected with the so called n-cycle scenario [58–61] quite the opposite happens: Nonsignaling correlations are generically classical. Second, by employing a recently introduced measure of nonlocality based on the trace distance [62], we consider a number of different Bell scenarios (with increasing number of outcomes, measurements, and parts) and numerically obtain the distribution of such a nonlocality quantifier over uniformly sampled NS correlations. In most cases, and perhaps not surprisingly, we obtain that the volume of the local set decays very fast with an increasing number of settings, outcomes, or parts. However, by considering the trace distance distribution of such nonlocal points to the local set, we have found that some interesting concentration phenomena can take place.

The paper is organized as follows. Section II introduces the basic framework and provides an overview of the results. In Secs. III and IV we provide analytical results regarding two scenarios where we only take into account the full correlations produced in the experiment. More precisely, in Sec. III we analyze a bipartite Bell scenario with an increasing number of measurements per party and in Sec. IV we study the geometry of correlations in the cycle scenario [58–61]. Section V discusses the distribution of the nonlocality measure introduced in [62] in a variety of Bell scenarios and notes the emergence of concentration phenomena. Finally, we discuss our results as well as potential venues for future work in Sec. VI.

II. PRELIMINARIES AND AN OVERVIEW OF THE RESULTS

Throughout the paper, we will consider the paradigmatic Bell scenario defined as

$$\Gamma := (N, m, d), \tag{1}$$

where N distant parts perform m different d-outcome measurements on their shares of a joint physical system. Initially, we restrict our attention to a bipartite scenario (with straightforward generalization to more parts) where $N = 2$ parts, Alice and Bob, perform measurements labeled by the variables x and y obtaining measurement outcomes described by the variables a and b, respectively, as shown in Fig. 1.

Assuming we do not have access to the internal mechanism of each box, our best description of the scenario is therefore

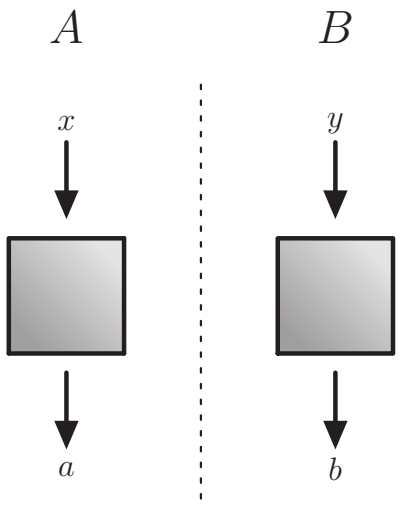

FIG. 1. Bipartite Bell scenario where two agents, Alice and Bob, share a pair of correlated measurement devices, whose inputs are labeled by x and y and outputs by a and b, respectively.

given by the joint statistics

$$\mathbf{p} := \{p(a, b|x, y)\},$$

that is, a list containing the probability $p(a, b|x, y)$ of obtaining outcomes a and b given that the parts have measured x and y. In a classical description, based on the assumption of local realism, such correlations can be decomposed as

$$p_{\mathrm{C}}(a, b|x, y) = \sum_{\lambda} p(\lambda) p(a|x, \lambda) p(b|y, \lambda). \tag{2}$$

This so-called local-hidden-variable description implies that all the correlations between Alice and Bob are assumed to be mediated by a common hidden variable λ that thus suffices to compute the probabilities of each of the outcomes, that is, $p(a|x, y, b, \lambda) = p(a|x, \lambda)$ (and similarly for b).

However, as discovered by Bell, there exist quantum correlations that do not comply with such a classical description. More precisely, local measurements on entangled states described by a density operator ρ give rise to probability distribution

$$p_{\mathrm{Q}}(a, b|x, y) = \mathrm{Tr}\left[\left(M_a^x \otimes M_b^y\right)\rho\right] \tag{3}$$

that might violate Bell inequalities, thus precluding its explanation by local-hidden-variable models.

Due to spatial distance, we do expect that outcomes of a given part are independent of the measurement choice of the other. This implies that the linear constraints

$$p(a|x) = \sum_b p(a, b|x, y) = \sum_b p(a, b|x, y'), \tag{4}$$

$$p(b|y) = \sum_a p(a, b|x, y) = \sum_a p(a, b|x', y), \tag{5}$$

known as nonsignaling conditions, must hold true. Interestingly, there are NS correlations beyond what we can achieve with quantum mechanics [37,38], that is, relativistic causality alone is not enough to single out the set of quantum correlations.

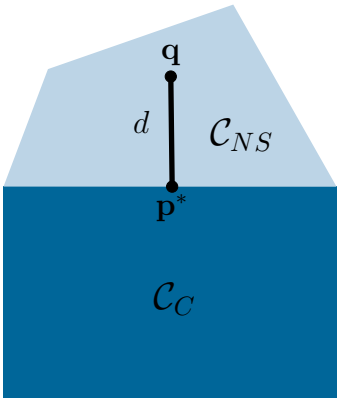

FIG. 2. Schematic drawing of a correlation $\mathbf{q} \in \mathscr{C}_{\mathrm{NS}}$ and $d = \mathrm{NL}(\mathbf{q})$, the distance (with respect to the ℓ_1-norm) from $\mathbf{q}$ to the closest local correlation $\mathbf{p}^* \in \mathscr{C}_C$.

Denoting the set of classical, quantum, and nonsignaling correlations by $\mathscr{C}_{\mathrm{C}}$, $\mathscr{C}_{\mathrm{Q}}$, and $\mathscr{C}_{\mathrm{NS}}$, respectively, a fundamental result in the study of nonlocality is the strict inclusion relations

$$\mathscr{C}_{\mathrm{C}} \subset \mathscr{C}_{\mathrm{Q}} \subset \mathscr{C}_{\mathrm{NS}}. \tag{6}$$

Strikingly, however, is the fact that apart from these strict inclusions there are only a few aspects known about the relation of these three sets of correlations. To mitigate that we employ here two different approaches that give us further insights into these sets of correlations.

First, we will be interested in the relative volumes between the sets. We identify two scenarios of interest with very different features. Considering a bipartite Bell scenario with an increasing number of measurement choices, we show analytically that generally the set of correlations is quantum and nonlocal. That is, at the same time that the volume of the local set shrinks, the quantum and NS sets become arbitrarily close. In contrast, considering the cycle scenario, again with an increasing number of possible measurements, we show that the volume of local correlations tends to unity, thus collapsing all the sets.

Arguably, however, the relative-volume method does not reveal the full picture of what really happens with the set of correlations. Classifying each correlation as either local or nonlocal is only a good indicator of what really happens with those sets. By considering our second figure of merit, we show that this is indeed the case. Not only have we decided whether a given correlation is nonlocal, but we have also quantified its degree of nonlocality. In doing so, we employ a measure given by [62]

$$\begin{aligned}\mathrm{NL}(\mathbf{q}) &= \frac{1}{|x||y|} \min_{\mathbf{p}\in\mathscr{C}_{\mathrm{C}}} D(\mathbf{q},\mathbf{p}) \\ &= \frac{1}{2|x||y|} \min_{\mathbf{p}\in\mathscr{C}_{\mathrm{C}}} \sum_{a,b,x,y} |q(a,b|x,y) - p(a,b|x,y)| \end{aligned} \tag{7}$$

to quantify the nonlocality of a given correlation $\mathbf{q} = q(a,b|x,y)$. This is the minimum trace distance between the correlation under test and the set of local correlations. Geometrically it should be understood (see Fig. 2) as how far a given decorrelation is from the local polytope defining the correlations (2), with the quantitative aspect that the degree of nonlocality of $\mathbf{q}$ that is equal to zero if and only if $\mathbf{q}$ is local. Beyond its geometrical and quantitative content, we point out that this distance has computational and numerical appeal, as it can be evaluated efficiently via a linear program [62].

Considering a number of different scenarios, we have uniformly sampled over the NS correlations and computed the distance of each sampled correlation to the set of local correlations. Our numerical findings go with our analytical results described above, by indicating that indeed there is an unexpectedly rapid convergence. For the $(2, m, 2)$ and $(N, 2, 2)$ scenarios our numerics indicate that while the relative size of the local set shrinks very fast (with an increasing number of measurements and parts, respectively), a concentration phenomenon takes part and it keeps nonlocal points at a distance, which increases with m and N, from the local set. For the cycle we observe a concentration of the volume close to the local set. Finally, for the $(2, 2, d)$ scenarios with $d = 3$ and 4 our numerics offer two different venues for further investigation: Either the volume of the local set increases with d, contrary to what happens with the other scenarios, or its volume decreases and shows a strong concentration phenomenon around it.

III. WHEN NONSIGNALING CORRELATIONS CAN BE GENERICALLY QUANTUM AND NONLOCAL

In this section we discuss both analytically and numerically how nonsignaling correlations can generically be quantum and nonlocal. For showing so, we explore the relative behavior between the local and the quantum sets of correlations with respect to the nonsignaling set for Bell scenarios Γ composed by two parts, m measurements for each part and two possible outputs for each chosen measurement, *i.e.*,

$$\Gamma = (2, m, 2). \tag{8}$$

In addition, rather than use directly the set of correlations $\{p(a,b|x,y)\}$ as we have introduced in the preceding section, it will be crucial for our findings to translate from that probability distribution parlance to the correlator language. Therefore, assuming without loss of generality that the labels of the outcomes belong to the set $\{\pm 1\}$, in this section we will only consider the objects

$$\begin{aligned}\tau_{x,y} &:= \langle x \cdot y \rangle = p(11|xy) + p(-1-1|xy) \\ &\quad - p(1-1|xy) - p(-11|xy), \end{aligned} \tag{9}$$

$$\alpha_x := \langle x \rangle = p(1|x) - p(-1|x), \tag{10}$$

$$\beta_y := \langle y \rangle = p(1|y) - p(-1|y) \tag{11}$$

for each pair of measurements $x, y \in [m]$. Although it is usual to call the matrices as in Eq. (11) full-correlation matrices, we will also interchangeably use the term correlation matrix to match our nomenclature with that in Refs. [53,63], which we have followed to obtain our analytical results. Actually, while these results will mostly focus on a representative subset of the full-correlation description of a Bell scenario (see Sec. III B 1), the reader should also note that our numerical findings (see Secs. III B 3 and III B 2) evidence that the same

conclusions for the local set also hold true in the complete description of the $(2, m, 2)$ scenario.

A. Preliminaries

Plugging the explicit expression of classical and quantum correlations in Eq. (11), one can justify our following definitions of local and quantum correlation matrices.

Definition 1. We say that a full-correlation matrix τ is classical or local whenever there is a probability space $(\Omega, \mathbb{P})$ and response functions A_x and B_y with $A_x(\omega), B_y(\omega) \in \{-1, +1\}$ for all $\omega \in \Omega$ satisfying

$$\tau_{x,y} = \int_\Omega A_x(\omega) B_y(\omega) d\mathbb{P}(\omega). \tag{12}$$

We denote the set of all such classical matrices by $\mathscr{C}$.

Definition 2. We say that τ is quantum whenever there exist Hilbert spaces H_A and H_B, a density operator ρ acting on $H_A \otimes H_B$, and two families of self-adjoint operators acting on H_A and H_B, respectively, with $\max_{x,y}\{\|A_x\|, \|B_y\|\} \leqslant 1$, such that

$$\tau_{x,y} = \mathrm{tr}[(A_x \otimes B_y)\rho]. \tag{13}$$

We denote the set of all such quantum matrices by $\mathscr{Q}$.

Roughly speaking, the next two objects we are about to describe, namely, $\|\cdot\|_{\ell_\infty^n \otimes_\pi \ell_\infty^n}$ the projective norm and $\gamma_2(\cdot)$ the γ_2-norm, are the most important objects within our framework. We refer to [53] for all details, but the reason why we are interested in these norms in the context of correlators is due to their power in signaling the underlying content of a given full-correlation matrix τ.

Definition 3. The projective tensor norm on $\mathbb{R}^n \otimes \mathbb{R}^n$ is defined as

$$\|\tau\|_{\ell_\infty^n \otimes_\pi \ell_\infty^n} := \inf\left\{\sum_{k=1}^n \|x_k\|_\infty \|y_k\|_\infty : \tau = \sum_{i=1}^n x_k \otimes y_k\right\}, \tag{14}$$

where τ is a matrix of size $n \times n$ viewed as an element of $\mathbb{R}^n \otimes \mathbb{R}^n$

Definition 4. Let τ be a real $n \times n$ matrix. We define its γ_2-norm as

$$\gamma_2(\tau) := \inf\{\|X\|_{\ell_2 \to \ell_\infty^n} \|Y\|_{\ell_1^n \to \ell_2} : \tau = XY\}, \tag{15}$$

where, denoting by $R_i(X)$ the ith row of an $n \times m$ matrix X and by $C_j(Y)$ the jth column of an $m \times n$ matrix Y, we have[1]

$$\begin{aligned} \|X\|_{\ell_2 \to \ell_\infty^n} &:= \max_{i \in [n]} \|R_i(X)\|_2, \\ \|Y\|_{\ell_1^n \to \ell_2} &:= \max_{j \in [n]} \|C_j(Y)\|_2. \end{aligned} \tag{16}$$

The relation between the local and the quantum set with the norms mentioned previously being given by the following set of lemmas [53].

Lemma 1. Let $\tau \in \mathbb{M}_n(\mathbb{R})$ represent a full-correlation matrix. Then the following two statements hold true: (a) $\tau \in \mathscr{C} \iff \|\tau\|_{\ell_\infty^n \otimes_\pi \ell_\infty^n} \leqslant 1$ and (b) $\tau \in \mathscr{Q} \iff \gamma_2(\tau) \leqslant 1$.

Lemma 2. Let T be an $n \times n$ random matrix with a biorthogonally invariant distribution[2] and assume that, with high probability,

$$\exists\, r > 0, \quad \|T\|_\infty \leqslant \frac{r + o(1)}{n} \|T\|_1 \quad \text{as } n \to \infty. \tag{17}$$

Then with high probability

$$\|T\|_{\ell_\infty^n \otimes_\pi \ell_\infty^n} \geqslant \left(\sqrt{\frac{16}{15}} - o(1)\right) \gamma_2(T) \quad \text{as } n \to \infty \tag{18}$$

so that defining

$$\tau := \frac{T}{\gamma_2(T)} \tag{19}$$

guarantees that it is quantum and is not classical as $n \to \infty$ with high probability.

Lemma 3. Let T be a random matrix with a biorthogonally invariant distribution which fulfills Eq. (17) above. Then we have

$$\gamma_2(T) = [1 \pm o(1)] \frac{\|T\|_1}{n}. \tag{20}$$

Remark. On the one hand, Lemma 1 says that when we view the set of correlation matrices as a subset of $\mathbb{M}_n(\mathbb{R})$, then it is the unitary ball defined by $\|\cdot\|_{\ell_\infty^n \otimes_\pi \ell_\infty^n}$ that determines whether a given correlation matrix is classical. On the other hand, the second part of the lemma guarantees that it is another unitary ball, now defined by the γ_2-norm, that dictates whether or not a given correlation matrix belongs to the quantum set. Both norms work therefore as a mechanism to determine the nature of a given matrix. Despite being very technical, Lemmas 2 and 3 can both be used to discuss the asymptotic behavior of correlations matrices for the $(2, m, 2)$ scenario.

B. Nonsignaling correlations are generically quantum

1. Asymptotic results

Since we are interested in scenarios in which the number n of inputs is greater than 1, it is possible to restate Lemma 3 above in a weaker version, more suitable for our purposes though.

Proposition 1. Let T be an $n \times n$ random matrix with a biorthogonally invariant distribution and assume that, with high probability,

$$\exists\, r > 0, \quad \|T\|_\infty \leqslant \frac{r + o(1)}{n^2} \|T\|_1 \quad \text{as } n \to \infty. \tag{21}$$

[1]For the sake of completeness let us make clear that ℓ_∞^n is the space of n-tuples together with the $\|\cdot\|_\infty$ norm and that analogously ℓ_1^n is also the space of n-tuples but now together with the $\|\cdot\|_1$ norm.

[2]A random matrix is said to have a biorthogonally invariant distribution whenever its probability distribution does not change when we multiply it by any orthogonal matrix, either from the right or from the left. Notice that it includes important subclasses of random matrices, for instance, Gaussian matrices and those which are Haar distributed.

Then with high probability

$$\gamma_2(T) = \frac{(1 \pm o(1))}{n^2}\|T\|_1. \tag{22}$$

Now suppose we are focused only on those full-correlation matrices τ which are nonsignaling. In that case we have

$$\begin{aligned}\|\tau\|_\infty = 1 &\leqslant [1 + o(1)]\frac{n^2}{n^2} \\ &= [1 + o(1)]\frac{\|\tau\|_1}{n^2}.\end{aligned} \tag{23}$$

Therefore, in addition, according to Proposition 1, we know that with high probability

$$\begin{aligned}\gamma_2(\tau) = \frac{1 \pm o(1)}{n^2}\|\tau\|_1 \leqslant \frac{1 + o(1)}{n^2}\|\tau\|_1 \leqslant \frac{1 + o(1)}{n^2}n^2 \\ = 1 + o(1),\end{aligned} \tag{24}$$

which in turns imply that if we know beforehand that a given full-correlation matrix τ belongs to the nonsignaling set, then with high probability it also belongs to the quantum set of correlations. Summing up, we state the following.

Proposition 2. As the number of inputs goes to infinity, nonsignaling full-correlation matrices (with a biorthogonal invariant distribution) are generically quantum.

Since in Ref. [53] the authors have found (see Lemma 2) that quantum full-correlation matrices are generically nonclassical, we can go even further. Once again, we can restate their main theorem, changing only the condition on flatness of the spectrum of τ, in order to obtain the following.

Proposition 3. Let T be an $n \times n$ random matrix with a biorthogonally invariant distribution and assume that, with high probability,

$$\exists\, r > 0, \quad \|T\|_\infty \leqslant \frac{r + o(1)}{n^2}\|T\|_1 \quad \text{as } n \to \infty. \tag{25}$$

Then with high probability

$$\|T\|_{\ell_\infty^n \otimes_\pi \ell_\infty^n} \geqslant \left(\sqrt{\frac{16}{15}} - o(1)\right)\frac{\|T\|_1}{n^2} \quad \text{as } n \to \infty. \tag{26}$$

With that result in hands, assuming that the τ is a random full-correlation matrix belonging to the nonsignaling set one has

$$\|T\|_{\ell_\infty^n \otimes_\pi \ell_\infty^n} \geqslant \left(\sqrt{\frac{16}{15}} - o(1)\right) \quad \text{as } n \to \infty, \tag{27}$$

which in turns shows that generically nonsignaling correlations do not belong to the set of classical correlations. Summing up, we have the following proposition.

Proposition 4. As the number of inputs goes to infinity, nonsignaling full-correlation matrices (with a biorthogonal invariant distribution) are generically nonclassical.

Giving to the reader a less abstract glimpse of our findings, we finish the present section by discussing numerically what happens with the distance distribution for nonlocal correlations in many different $(2, m, 2)$ scenarios.

TABLE I. Volume of the classical set in the $(2, m, 2)$ scenario with the Gibbs sampler within the MATLAB function `crpnd` for $m = 2, 3, 4, 5$. The second column shows the number of points sampled, No. L denotes the number of local points found (within numerical precision of 10^{-10}), and % L denotes the ratio between the number of local points and the number of nonsignaling points.

m	10^x	No. L	% L
2	7	9414201	94.14
3	6	621123	62.11
4	6	212093	21.20
5	6	37396	3.73

2. *Numerical results for the* $(2, m, 2)$ *Bell scenario*

We now analyze what happens when we estimate the relative volume of the classical set when considering the complete correlation

$$(\langle x\rangle, \langle y\rangle, \langle xy\rangle). \tag{28}$$

To do so we (i) used the Gibbs sampler within the MATLAB function `cprnd` as implemented by Benham [64] to (ii) generate a set of uniformly distributed points in $\mathbf{q} \in \mathscr{C}_{\mathrm{NS}}$ and (iii) then compute NL($\mathbf{q}$). Table I summarizes our results. The case $m = 2$ corresponds to the usual Clauser-Horne-Shimony-Holt scenario, and what we have found coincides with the results of Refs. [50,51], which are however based upon other methods. The volume of the classical set decreases fast with m, as we can see in Fig. 3(a). Note, however, that the decaying in the

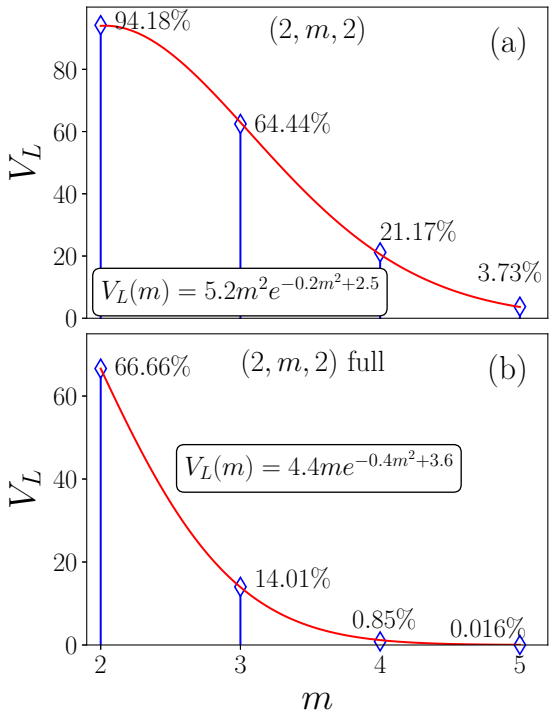

FIG. 3. (a) Relative volume $V_{\mathrm{L}}/V_{\mathrm{NL}}$ for the $(2, m, 2)$ Bell scenario. (b) Relative volume $V_{\mathrm{L}}/V_{\mathrm{NL}}$ for the $(2, m, 2)$ Bell scenario with only full correlators. In both cases the relative volume of the local set decreases with m; however, for the full correlators scenario the volume decreases faster. The red line is the best fit we numerically find for these points.

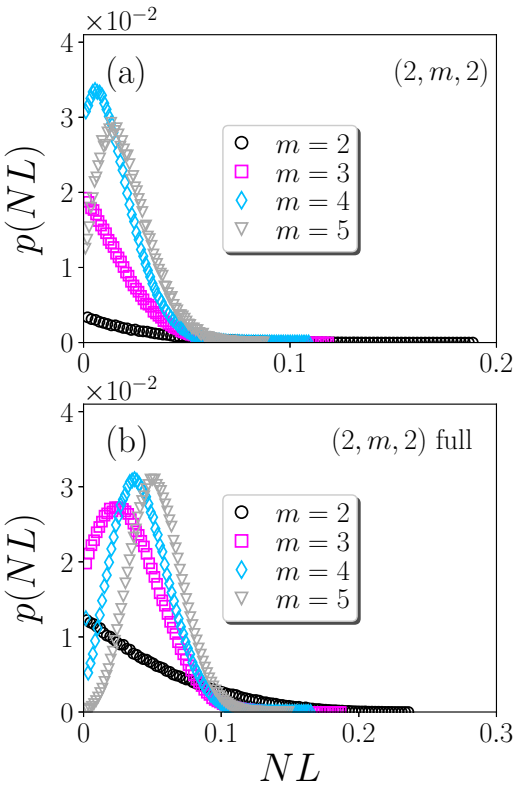

FIG. 4. Distance distribution for the nonlocal correlations in the Bell scenario with 10^6 samples. (a) The $(2, m, 2)$ Bell scenario for $m = 2, 3, 4, 5$. (b) The $(2, m, 2)$ Bell scenario where only full correlators are considered for $m = 2, 3, 4, 5$. The numerical precision is within 10^{-10}. We are considering local correlations for the result $\mathrm{NL}(\mathbf{q}) \leqslant 10^{-10}$ and nonlocal otherwise.

volume ratio is much more notable in the scenario where only full correlators are considered, thus showing the relevance of marginal information in the geometry of the Bell correlations.

As in the case with full correlators only (see Sec. III B 3), the probability of finding a point at distance l from the local set does not decrease monotonically with l, except for $m = 2$. For $m = 2$, each nonlocal extremal point violates only one facet-defining Bell inequality and hence the nonlocal portion of the nonsignaling set consists of disjoint pyramids whose apex is one of the nonlocal extremal points and the basis is a simplex whose vertices are the local extremal points saturating the corresponding inequality. This is no longer the case for $m > 2$, where there are correlations that might violate more than one facet-defining inequality. The nonsignaling and classical sets have a much more complicated geometry in this case, which manifests as the nonmonotonic behavior of the trace distance shown in Fig. 4(a).

3. Numerical results for the full-correlation $(2, m, 2)$ *Bell scenario*

In the full-correlation framework, the nonsignaling set for the $(2, m, 2)$ scenario is the hypercube $\{-1, 1\}^{m^2}$. To estimate the relative volume of the classical set we sample uniformly from this hypercube and calculate the trace distance $\mathrm{NL}(\mathbf{q})$. We summarize our findings in Table II. These results show

TABLE II. Volume of the classical set in the full-correlation $(2, m, 2)$ scenario. From a total of 10^6 sampled points, No. L denotes the number of local points found (within numerical precision of 10^{-10}) and % L denotes the ratio between the number of local points and the number of nonsignaling points.

m	No. L	% L
2	666657	66.66
3	140138	14.01
4	8470	0.847
5	165	0.016

that the volume of the local set decreases rapidly as m grows, supporting the analytical results obtained in the preceding section.

The distance distribution for the nonlocal full correlators for $m = 2, 3, 4, 5$ is shown in Fig. 4(b), and in Fig. 3(b) we can see how the relative volume of the local set decreases with m. The probability of finding a point at distance l from the local set decreases monotonically with l only for $m = 2$. For $m > 2$ we have the emergence of a concentrationlike phenomenon, where the distribution shows a peak that moves to the right with increasing m. That is, not only does the volume of the local set decrease fast, but most of the nonlocal points are concentrated at a certain distance that increases with the number of measurement settings m. Clearly, we have here a signature of the complicated geometry of Bell correlations.

IV. NONSIGNALING CORRELATIONS CAN BE GENERICALLY LOCAL

Here we will give an example of a scenario where the relative volume of the set of local correlations tends to unity. The scenario in question is known as the cycle scenario: We have n measurements $x_1, \ldots, x_n$ for the first party and n measurements $y_1, \ldots, y_n$ for the second party, with binary outputs ± 1. We consider only the joint distributions for x_i and y_j whenever $i - j = 1 \bmod n$. Similarly to a usual Bell scenario, the cycle scenario is described by the probability distributions

$$p(a_i b_j | x_i y_j) \tag{29}$$

for $i - j = 1 \mod n$.

In what follows we will analytically compute the volume of local and nonsignaling sets as a function of n and show that $V_{\mathrm{L}}/V_{\mathrm{NS}} \to 1$. It is crucial for our construction to consider exclusively the full correlators $\langle x_i y_j \rangle$. However, at the end of the section we will provide evidence indicating that the same result holds also considering the complete probability distributions.

In the full-correlation framework, the nonsignaling set is the hypercube $\{-1, 1\}^{2n}$ with 2^{2n} vertices, 2^{2n-2} of them nonlocal (odd number of entries equal to -1) and the other 2^{2n-1} corresponding to local ones (even number of entries equal to -1) [61]. Each nonlocal extremal point violates only one facet-defining Bell inequality and hence the nonlocal portion of the nonsignaling set consists of 2^{2n-1} disjoint pyramids, whose apex is one of the nonlocal extremal points and the basis is a simplex in dimension $2n - 1$ whose vertices

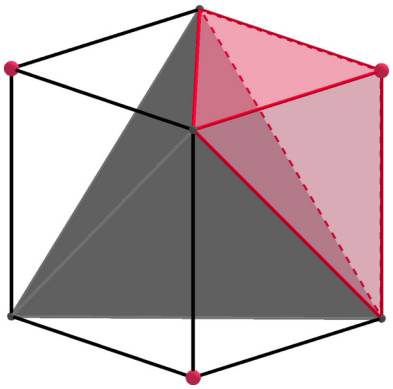

FIG. 5. Schematic representation of the set of nonsignaling correlations in the cycle scenario. The small vertices represent the local vertices, whose convex rule gives the local set. The big vertices represent the nonlocal vertices. Notice that the nonlocal part of the nonsignaling set corresponds to disjoint pyramids, one of which is shown lightly shaded.

are the $2n$ local extremal points saturating the corresponding inequality. Thus, the volume of the local set is the volume of the hypercube minus the volume of these pyramids. A schematic representation of this set is shown in Fig. 5.

Remembering basic geometry, we know that to calculate the volume of one of these pyramids we need to know the area of the basis and the height. First, we calculate the area of the basis. The volume of a simplex with $v+1$ vertices and side s is equal to

$$V_S = \frac{s^v}{v!}\sqrt{\frac{v+1}{2^v}}. \tag{30}$$

The basis of the pyramid is a simplex with $2n$ vertices and side $\sqrt{8}$, the Euclidean distance from two adjacent vertices of the local polytope. Hence, its area is given by

$$A_B = \frac{\sqrt{8}^{2n-1}}{(2n-1)!}\sqrt{\frac{2n}{2^{2n-1}}}. \tag{31}$$

In turn, the height of the pyramid is the Euclidean distance of the nonsignaling extremal point to the uniform convex mixture of the local ones and is given by

$$h = \frac{2}{\sqrt{2n}}. \tag{32}$$

We can now calculate the volume of the pyramid simply as

$$V_P = \frac{h \times A_B}{2n} = \frac{2^{2n}}{(2n)!}. \tag{33}$$

Since we have 2^{2n-1} such pyramids, the total volume will be

$$V_L = 2^{2n} - 2^{2n-1} \times \frac{2^{2n}}{(2n)!} = 2^{2n}\left(1 - \frac{2^{2n-1}}{(2n)!}\right). \tag{34}$$

Clearly, with $n \to \infty$ the volume of the local set tends to the volume of the hypercube and thus $V_{\mathrm{L}}/V_{\mathrm{NS}} \to 1$. As can be seen from Table III, the relative volume of the local set tends very rapidly to unity and already at $n = 4$ it achieves approximately 0.997.

To complete the picture of the cycle with full correlators, we have uniformly sampled inside the nonsignaling set and computed the distance to the set of local correlations. The results are shown in Fig. 6.

Finally, we have also computed the distribution of the trace distance taking into account a uniform sampling over the complete probability distribution. We use two different methods to sample the points from the nonsignaling set. The first step in both methods is to write the probability distribution in terms of expectation values

$$\langle x_i \rangle = p(1|x_i) - p(-1|x_i), \tag{35}$$

$$\langle y_j \rangle = p(1|y_j) - p(-1|y_j), \tag{36}$$

$$\begin{aligned}\langle x_i y_j \rangle = {} & p(11|x_i y_j) + p(-1-1|x_i y_j) \\ & - p(-11|x_i y_j) - p(1-1|x_i y_j).\end{aligned} \tag{37}$$

The map that takes each nonsignaling probability in the vector

$$(\langle x_i \rangle, \langle y_j \rangle, \langle x_i y_j \rangle), \tag{38}$$

with $i - j = 1 \mod n$, is bijective and gives a full-dimensional parametrization of the nonsignaling set in $\mathbb{R}^{4n}$. Further, notice that the image of the nonsignaling set under this map belongs to the hypercube $[-1, 1]^{4n}$. A point in the

TABLE III. Volume of the set of local correlators in the cycle scenario for $n = 2, 3, 4$. The first column shows the value of n. Columns 2 and 3 show the number of full-correlation local points No. L and the percentage of full-correlation local points % L, respectively, from a sample of 10^6 points for every n. The data obtained when we sample considering the entire correlation with methods M1 (sampling over the hypercube and discarding the signaling points) and M2 (sampling directly over the NS polytope using the MATLAB `cprnd` function) are shown in columns 4–10. Columns 4–8 show the number of points No. P sampled, the number of nonsignaling points No. NS, the number of local points No. L, the percentage of nonsignaling points % NS and the percentage of local points % L obtained with method M1. Columns 9 and 10 show the number of local points No. L and the percentage of local points % L, respectively, from a sample of 10^6 points, obtained with method M2.

	Full		Complete M1					Complete M2	
n	No. L	% L	No. $P = 10^x$	No. NS	No. L	% NS	% L	No. L	% L
2	666362	66.7	7	268896	253061	2.69	94.11	939828	93.98
3	955538	95.6	8	442814	442589	0.44	99.95	999617	99.96
4	996816	99.7	9	727331	727328	0.07	100	999997	∼100

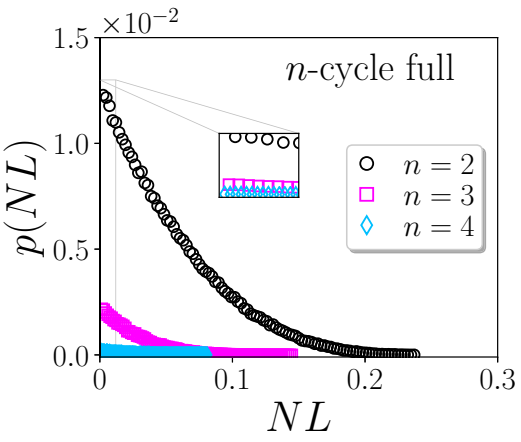

FIG. 6. Distance distribution for the contextual full correlators in the n-cycle scenario for $n = 2, 3, 4$ and 10^6 samples. The numerical precision is within of 10^{-10}. We are considering local correlations for the result $\mathrm{NL}(\mathbf{q}) \leqslant 10^{-10}$ and nonlocal otherwise.

hypercube belongs to the image of the nondisturbing set if it satisfies

$$p(a_i b_j|x_i y_j) = \frac{1 + a_i\langle x_i\rangle + b_j\langle y_j\rangle + a_i b_j\langle x_i y_j\rangle}{4} \geqslant 0 \quad (39)$$

for all $a, b = \pm 1$ and $i - j = \mathrm{mod}\, n$. In the first method, we sample uniformly from the hypercube $[-1, 1]^{4n}$, test if inequalities (39) are satisfied, and discard the points that are outside the image of the nonsignaling set. Then we compute the distance of this point to the local set. The results are shown in Table III. Notice that this method is very inefficient because the relative volume of the nonsignaling set with respect to the hypercube is very small. Nevertheless, it offers a good testing ground for other methods since we are sure that the sampling is indeed uniform.

In the second method we use the Gibbs sampler within the MATLAB function `cprnd` [64]. The results are shown in Table III and agree with the results obtained with the previous method. The volume of the local set grows with n, showing the same behavior as in Fig. 6.

The probability of finding a point at distance D from the local set decreases monotonically with D. This is a signature of the geometry of the nonsignaling set. Again, in this scenario, each nonlocal extremal point violates only one facet-defining Bell inequality and hence the nonlocal portion of the nonsignaling set consists of disjoint pyramids whose apex is one of the nonlocal extremal points and the basis is a simplex whose vertices are the local extremal points saturating the corresponding inequality.

V. CONCENTRATION PHENOMENA OF NONLOCAL CORRELATIONS

So far we have focused on a bipartite scenario where the number of measurements increases but the number of outcomes is always two. In the following we show that while similar results hold true when we increase the number of parts, keeping dichotomic measurements, they can change dramatically if instead we keep fixed the number of parts and measurements and increase the number of measurement outcomes.

TABLE IV. Volume of the local set in the correlation $(N, 2, 2)$ scenario.

N	No. NS $= 10^x$	No. L	% L
2	7	9414201	94.14201
3	6	585206	58.52
4	6	40576	4.06

A. The $(N, 2, 2)$ Bell scenario

In the $(N, 2, 2)$ Bell scenario N parts have each two binary measurements. To find a full-dimensional parametrization of $\mathscr{C}_{\mathrm{NS}}$ we write the correlations in terms of the probabilities

$$p(-1|x_i), \quad p(-1-1|x_i x_j),$$
$$p(-1-1-1|x_i x_j x_k), \quad p(-1-1\cdots-1|x_1 x_2 \cdots x_N). \quad (40)$$

We can recover every probability $p(a_1 \cdots a_N|x_1 \cdots x_N)$ from the vector with entries given by Eqs. (40). Hence, the map that takes each correlation to the corresponding vector (40) is bijective and gives a full-dimensional parametrization of the nonsignaling set. Notice that the image of the nonsignaling set under this map belongs to the hypercube with coordinates in [0,1]. A point in the hypercube belongs to the image of the nonsignaling set if every $p(a_1 \cdots a_N|x_1 \cdots x_N)$ recovered from it is positive.

To estimate the relative volume of the local set we use the Gibbs sampler within the `crnpd` MATLAB function and calculate trace distance NL. The results are shown in Table IV. The distance distribution for the nonlocal correlations for $N = 2, 3, 4$ is shown in Fig. 7(a).

B. Full-correlation $(N, 2, 2)$ Bell scenario

Also in the $(N, 2, 2)$ scenario we can describe the correlations using only full correlations $\langle x_1 x_2 \cdots x_N\rangle$. In this framework, the nonsignaling set is the hypercube $\{-1, 1\}^{2^N}$.

To estimate the relative volume of the local set we sample uniformly from the hypercube and calculate the trace distance NL. The results are shown in Table V.

The distance distribution for the nonlocal correlations for $N = 2, 3, 4$ is shown in Fig. 7(b). As in the $(2, m, 2)$ scenario, the volume of the local set decays more rapidly when only the full correlators are considered (in comparison with when the marginal information is taken into account). Again, the nonlocal points are concentrated at a distance that increases as we increase the number of parts n.

C. The $(2, 2, d)$ Bell scenario

In the $(2, 2, d)$ Bell scenario Alice and Bob have each two d-outcome measurements. The set of nonsignaling correlations is a $4(d^2 - d)$-dimensional set in $\mathbb{R}^{4d^2}$. In order to perform the sampling in $\mathscr{C}_{\mathrm{NS}}$, we need to find a full-dimensional parametrization of $\mathscr{C}_{\mathrm{NS}}$ in $\mathbb{R}^{4(d^2-d)}$. In this case,

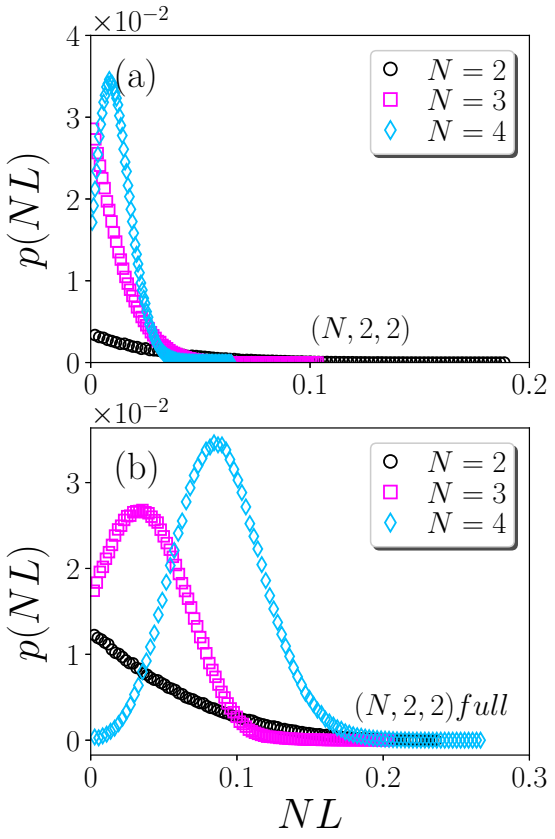

FIG. 7. Distance distribution for the nonlocal correlations in the Bell scenario with 10^6 samples. (a) The $(N, 2, 2)$ Bell scenario for $N = 2, 3, 4$. (b) The $(N, 2, 2)$ Bell scenario where only full correlators are considered for $N = 2, 3, 4$. The numerical precision is within of 10^{-10}. We are considering local correlations for the result $\mathrm{NL}(\mathbf{q}) \leqslant 10^{-10}$ and nonlocal otherwise.

we cannot use expectation values to describe the correlations and we have carefully chosen which probabilities $p(ab|xy)$ we will keep and which probabilities we will discard.

In this scenario it suffices to keep the probabilities $p(ab|xy)$ with $a = 0, \ldots, d-2$ and $b = 0, \ldots, d-1$ if $xy = 00$ or $xy = 11$ and the probabilities $p(ab|xy)$ with $a = 0, \ldots, d-1$ and $b = 0, \ldots, d-2$ if $xy = 01$ or $xy = 10$. All other probabilities $p(ab|xy)$ can be recovered from these using nonsignaling and normalization conditions. This gives a full-dimensional parametrization of $\mathscr{C}_{\mathrm{NS}}$ in $\mathbb{R}^{4(d^2-d)}$. The image of the nonsignaling set under this projection belongs to the hypercube $[0, 1]^{4(d^2-d)}$. A point in the hypercube belongs to the image of the nonsignaling set if every $p(ab|xy)$ recovered from it is positive.

TABLE V. Relative volume of the classical set in the full-correlation $(N, 2, 2)$ Bell scenario using a sample of 10^6 nonsignaling points.

N	No. L	% L
2	666657	66.66
3	102367	10.23
4	188	0.0188

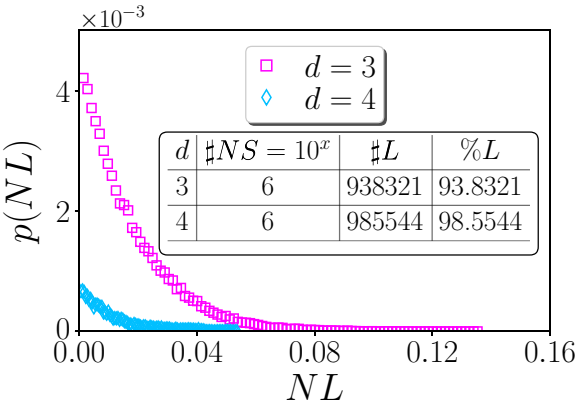

d	$\sharp NS = 10^x$	$\sharp L$	$\%L$
3	6	938321	93.8321
4	6	985544	98.5544

FIG. 8. Distance distribution for the nonlocal correlations in the $(2, 2, d)$ Bell scenario for $d = 3$ and 4.

To estimate the relative volume of the classical set we use the Gibbs sampler within the `crnpd` MATLAB function and calculate trace distance $\mathrm{NL}(\mathbf{q})$. The distance distribution for the nonlocal correlations for $d = 3, 4$ and the relative volumes are shown in Fig. 8.

Counterintuitively and contrary to the $(2, m, 2)$ and $(N, 2, 2)$ scenarios, apparently the volume of the local set is increasing and the concentration of the nonlocal points is very close to the local boundary. However, these results might be an artifact of the numerical precision. Our codes have a precision of 10^{-10} when computing the trace distance to the local set. That is, any nonlocal point with a distance below this threshold will count as local. This is not an issue in the $(2, m, 2)$ and $(N, 2, 2)$ scenarios because not only does the local set shrink, but also the distance to it increases.

Within our numerical precision, two opposite results become possible. In the first, the volume of the local set indeed and counterintuitively increases with d. The second option is that the local volume decreases but at the same time all the nonlocal points are concentrated at a very small distance from the local set and thus cannot be distinguished by our numerical precision. In either case, we believe that is a very interesting and nontrivial result.

VI. DISCUSSION

Nonlocality is an key concept in foundations of quantum physics and has also found practical applications. In both contexts, understanding the geometry of the nonsignaling, quantum, and local set is certainly an important primitive. Here we have studied their relative volumes and the distribution of a quantitative measure of nonlocality using both analytical and numerical methods.

We have found analytically two different classes of full-correlation Bell scenarios where the nonsignaling correlations can behave very differently: In the $(2, m, 2)$ scenario the correlations are generically quantum and nonlocal, while in the cycle scenario the correlations are generically classical and local. Our numerical findings show that a similar result holds true when the entire probability distribution (and not just the full correlators) is taken into account and also when considering the $(n, 2, 2)$ scenario with more parts.

The distribution of our chosen quantifier for nonlocality, based on the trace distance between the probability distribution under testing and the set of local correlations introduced in Ref. [62], has unveiled interesting features in various scenarios. Of particular relevance, we have seen that in the $(2, m, 2)$ and $(N, 2, 2)$ scenarios not only does the volume of the local set decrease very rapidly, but also the nonlocal points are concentrated at a distance from the local set that increases with both m and N. We believe that such a surprising behavior reflects the signature of the complicated geometry of the nonsignaling and local sets, giving further insight into the relation between local and nonsignaling set.

Regarding the $(2, 2, d)$ scenario, due to numerical precision, our results are inconclusive so far. Considering a precision of $\varepsilon = 10^{-10}$ in the calculation of the nonlocality quantifier $\mathrm{NL}(\mathbf{q})$, we have seen that the volume of points with $\mathrm{NL}(\mathbf{q}) \leqslant \varepsilon$ increases as we increase the number of outcomes d. Two options are available. First, the volume of the local set, as opposed to the other scenarios, increases with d. This is similar to the recent result obtained in [65], where it is shown that the probability of violation of a Bell inequality in $(2, d, 2)$ decreases with d if one considers a maximally entangled state and randomly sampled projective measurements. The second option is that the local volume is indeed decreasing (as intuition would suggest) but at the same time the distribution of $\mathrm{NL}(\mathbf{q})$ is concentrated at an ε distance from the local set. Either way, this shows the complex geometry of the Bell correlations and is a point that certainly deserves further investigation.

Finally, we highlight that even though here we have focused on Bell nonlocality, the same methods can also be applied not only to study the differences between classical and nonclassical resources in more general notions of nonlocality and contextuality, but also to study the relative volumes, in many different scenarios, between the classical set and those sets of correlations defined by the Navascués-Pironio-Acín hierarchy, as suggested by the authors in [66]. We hope our results might motivate further research in these directions.

ACKNOWLEDGMENTS

The authors acknowledge the Brazilian ministries MEC and MCTIC, funding agency CNPq (PQ Grant No. 307172/2017-1), INCT-IQ, the John Templeton Foundation via the grant Q-CAUSAL No. 61084 and the Serrapilheira Institute (Grant No. Serra-1708-15763). B.A. also thanks T. A. Jorge for the help with the MATLAB codes. C.D. was also supported by a fellowship from the Grand Challenges Initiative at Chapman University.

[1] J. S. Bell, Physics **1**, 195 (1964).
[2] A. K. Ekert, Phys. Rev. Lett. **67**, 661 (1991).
[3] J. Barrett, L. Hardy, and A. Kent, Phys. Rev. Lett. **95**, 010503 (2005).
[4] A. Acín, N. Gisin, and L. Masanes, Phys. Rev. Lett. **97**, 120405 (2006).
[5] U. Vazirani and T. Vidick, Phys. Rev. Lett. **113**, 140501 (2014).
[6] S. Pironio, A. Acín, S. Massar, A. B. de La Giroday, D. N. Matsukevich, P. Maunz, S. Olmschenk, D. Hayes, L. Luo, T. A. Manning, and C. Monroe, Nature (London) **464**, 1021 (2010).
[7] R. Colbeck and A. Kent, J. Phys. A: Math. Theor. **44**, 095305 (2011).
[8] D. Mayers and A. Yao, Quantum Inf. Comput. **4**, 273 (2004).
[9] O. Andersson, P. Badziąg, I. Bengtsson, I. Dumitru, and A. Cabello, Phys. Rev. A **96**, 032119 (2017).
[10] A. Coladangelo, K. T. Goh, and V. Scarani, Nat. Commun. **8**, 15485 (2017).
[11] N. Brunner, S. Pironio, A. Acin, N. Gisin, A. A. Méthot, and V. Scarani, Phys. Rev. Lett. **100**, 210503 (2008).
[12] K. F. Pál and T. Vértesi, Phys. Rev. A **96**, 022123 (2017).
[13] Y. Cai, J.-D. Bancal, J. Romero, and V. Scarani, J. Phys. A: Math. Theor. **49**, 305301 (2016).
[14] Č. Brukner, M. Żukowski, J.-W. Pan, and A. Zeilinger, Phys. Rev. Lett. **92**, 127901 (2004).
[15] H. Buhrman, R. Cleve, S. Massar, and R. de Wolf, Rev. Mod. Phys. **82**, 665 (2010).
[16] R. Chaves, D. Cavalcanti, L. Aolita, and A. Acín, Phys. Rev. A **86**, 012108 (2012).
[17] B. Hensen, H. Bernien, A. E. Dréau, A. Reiserer, N. Kalb, M. S. Blok, J. Ruitenberg, R. F. Vermeulen, R. N. Schouten, C. Abellan *et al.*, Nature (Lodon) **526**, 682 (2015).
[18] M. Giustina, M. A. Versteegh, S. Wengerowsky, J. Handsteiner, A. Hochrainer, K. Phelan, F. Steinlechner, J. Kofler, J.-A. Larsson, C. Abellan *et al.*, Phys. Rev. Lett. **115**, 250401 (2015).
[19] L. K. Shalm, E. Meyer-Scott, B. G. Christensen, P. Bierhorst, M. A. Wayne, M. J. Stevens, T. Gerrits, S. Glancy, D. R. Hamel, M. S. Allman *et al.*, Phys. Rev. Lett. **115**, 250402 (2015).
[20] W. Rosenfeld, D. Burchardt, R. Garthoff, K. Redeker, N. Ortegel, M. Rau, and H. Weinfurter, Phys. Rev. Lett. **119**, 010402 (2017).
[21] I. Pitowsky, Math. Program. **50**, 395 (1991).
[22] N. Brunner, D. Cavalcanti, S. Pironio, V. Scarani, and S. Wehner, Rev. Mod. Phys. **86**, 419 (2014).
[23] R. F. Werner and M. M. Wolf, Phys. Rev. A **64**, 032112 (2001).
[24] D. Collins, N. Gisin, N. Linden, S. Massar, and S. Popescu, Phys. Rev. Lett. **88**, 040404 (2002).
[25] D. Collins and N. Gisin, J. Phys. A: Math. Gen. **37**, 1775 (2004).
[26] S. Popescu, Phys. Rev. Lett. **74**, 2619 (1995).
[27] R. Gallego, L. E. Würflinger, R. Chaves, A. Acín, and M. Navascués, New J. Phys. **16**, 033037 (2014).
[28] B. F. Toner and D. Bacon, Phys. Rev. Lett. **91**, 187904 (2003).
[29] S. Pironio, Phys. Rev. A **68**, 062102 (2003).
[30] K. Maxwell and E. Chitambar, Phys. Rev. A **89**, 042108 (2014).
[31] R. Chaves, R. Kueng, J. B. Brask, and D. Gross, Phys. Rev. Lett. **114**, 140403 (2015).
[32] J. B. Brask and R. Chaves, J. Phys. A: Math. Theor. **50**, 094001 (2017).
[33] M. Ringbauer and R. Chaves, Quantum **1**, 35 (2017).
[34] R. Chaves, G. Carvacho, I. Agresti, V. Di Giulio, L. Aolita, S. Giacomini, and F. Sciarrino, Nat. Phys. **14**, 291 (2018).
[35] R. Chaves, Phys. Rev. Lett. **116**, 010402 (2016).

[36] D. Rosset, C. Branciard, T. J. Barnea, G. Pütz, N. Brunner, and N. Gisin, Phys. Rev. Lett. **116**, 010403 (2016).
[37] S. Popescu and D. Rohrlich, Found. Phys. **24**, 379 (1994).
[38] M. L. Almeida, J.-D. Bancal, N. Brunner, A. Acín, N. Gisin, and S. Pironio, Phys. Rev. Lett. **104**, 230404 (2010).
[39] W. van Dam, Nat. Comput. **12**, 9 (2013).
[40] M. Pawłowski, T. Paterek, D. Kaszlikowski, V. Scarani, A. Winter, and M. Żukowski, Nature (London) **461**, 1101 (2009).
[41] M. Navascués and H. Wunderlich, Proc. R. Soc. A **466**, 881 (2009).
[42] M. Navascués, Y. Guryanova, M. J. Hoban, and A. Acín, Nat. Commun. **6**, 6288 (2015).
[43] T. Fritz, A. B. Sainz, R. Augusiak, J. B. Brask, R. Chaves, A. Leverrier, and A. Acín, Nat. Commun. **4**, 2263 (2013).
[44] R. Chaves, C. Majenz, and D. Gross, Nat. Commun. **6**, 5766 (2015).
[45] A. Schrijver, *Theory of Linear and Integer Programming* (Wiley, New York, 1999).
[46] G. B. Dantzig and M. N. Thapa, in *Linear Programming 2: Theory and Extensions*, edited by P. W. Glynn and S. M. Robinson, Springer Series in Operations Research (Springer, New York, 2003).
[47] M. Navascués, S. Pironio, and A. Acín, Phys. Rev. Lett. **98**, 010401 (2007).
[48] M. Navascués, S. Pironio, and A. Acín, New J. Phys. **10**, 073013 (2008).
[49] K. T. Goh, J. Kaniewski, E. Wolfe, T. Vértesi, X. Wu, Y. Cai, Y.-C. Liang, and V. Scarani, Phys. Rev. A **97**, 022104 (2018).
[50] A. Cabello, Phys. Rev. A **72**, 012113 (2005).
[51] E. Wolfe and S. F. Yelin, Phys. Rev. A **86**, 012123 (2012).
[52] A. Canabarro, S. Brito, and R. Chaves, arXiv:1808.07069.
[53] C. E. González-Guillén, C. Lancien, C. Palazuelos, and I. Villanueva, Ann. Henri Poincaré **18**, 3793 (2017).
[54] C. E. González-Guillén, C. H. Jiménez, C. Palazuelos, and I. Villanueva, Commun. Math. Phys. **344**, 141 (2016).
[55] C. Palazuelos, Found. Phys. **48**, 857 (2018).
[56] R. C. Drumond, C. Duarte, and R. I. Oliveira, J. Math. Phys. **59**, 052202 (2018).
[57] D. Pérez-García, M. M. Wolf, C. Palazuelos, I. Villanueva, and M. Junge, Commun. Math. Phys. **279**, 455 (2008).
[58] S. L. Braunstein and C. M. Caves, Ann. Phys. (NY) **202**, 22 (1990).
[59] A. A. Klyachko, M. A. Can, S. Binicioglu, and A. S. Shumovsky, Phys. Rev. Lett. **101**, 020403 (2008).
[60] R. Chaves and T. Fritz, Phys. Rev. A **85**, 032113 (2012).
[61] M. Araujo, M. T. Quintino, C. Budroni, M. T. Cunha, and A. Cabello, Phys. Rev. A **88**, 022118 (2013).
[62] S. G. A. Brito, B. Amaral, and R. Chaves, Phys. Rev. A **97**, 022111 (2018).
[63] B. S. Tsirelson, Hadronic J. Suppl. **8**, 329 (1993).
[64] T. Benham, Uniform distribution over a convex polytope, MATLAB central file exchange, accessed 01-01-2018.
[65] A. Fonseca, A. de Rosier, T. Vértesi, W. Laskowski, and F. Parisio, Phys. Rev. A **98**, 042105 (2018).
[66] L. Yeong-Cherng *et al.* (private communication).